© 2020. Published by The Company of Biologists Ltd | Journal of Cell Science (2020) 133, jcs240358. doi:10.1242/jcs.240358

RESEARCH ARTICLE

# Detecting single ORAI1 proteins within the plasma membrane reveals higher-order channel complexes

**Dalia Alansary[1], Diana B. Peckys[1], Barbara A. Niemeyer[1,*] and Niels de Jonge[2,3,*]**

## ABSTRACT

ORAI1 proteins form highly selective $Ca^{2+}$ channels in the plasma membrane. Crystallographic data point towards a hexameric stoichiometry of ORAI1 channels, whereas optical methods postulated ORAI1 channels to reside as dimers at rest, and other data suggests that they have a tetrameric configuration. Here, liquid-phase scanning transmission electron microscopy (STEM) and quantum dot (QD) labeling was utilized to study the conformation of ORAI1 proteins at rest. To address the question of whether ORAI1 was present as a dimer, experiments were designed using single ORAI1 monomers and covalently linked ORAI1 dimers with either one or two label-binding positions. The microscopic data was statistically analyzed via the pair correlation function. Label pairs were found in all cases, even for concatenated dimers with one label-binding position, which is only possible if a significant fraction of ORAI1 was assembled in larger order oligomers than dimers, binding at least two QDs. This interpretation of the data was consistent with Blue Native PAGE analysis showing that ORAI1 is mainly present as a complex of an apparent molecular mass larger than that calculated for a dimer.

**KEY WORDS: $Ca^{2+}$ channel, ORAI1, Hexamer, Liquid-phase electron microscopy, Graphene, Pair correlation function**

## INTRODUCTION

Cellular communication requires detection of signals by surface receptors such as G-protein-coupled receptors, tyrosine kinase receptors or directly ligand-gated ion channels. Those surface receptors, coupling through activation of phospholipase C, generate cytosolic inositol (1,4,5)-trisphosphate ($IP_3$), which upon binding to its endoplasmic reticulum (ER) resident IP3 receptor (IP3R), lead to release of ER-stored $Ca^{2+}$ into the cytosol. The concomitant reduction of luminal $Ca^{2+}$ is sensed by STIM1 and its homolog STIM2, leading to their conformational change, oligomerization, and the accumulation of the partially unfolded proteins in ER–plasma membrane junctions. Here, STIM molecules bind and trap ORAI channels (ORAI1, ORAI2 or ORAI3) diffusing within the plasma membrane and directly gate them via interaction with their channel-activating domain [CAD or SOAR (Park et al., 2009; Yuan et al., 2009; reviewed in Prakriya and Lewis, 2015)]. The resulting store-operated $Ca^{2+}$ entry (SOCE) triggers multiple cellular pathways and activates transcription factors (Dolmetsch, 2003, reviewed in Bergmeier et al., 2013; Kar and Parekh, 2013). The duration and intensity of the original upstream stimulus affect the kinetics of SOCE and as a result, fine tune the intracellular $Ca^{2+}$ concentrations and downstream effector processes.

Clustering of STIM1 and its subsequent trapping, and clustering of ORAI proteins are rate-determining steps for the resulting $Ca^{2+}$ influx. Furthermore, the ratio of STIM1 to ORAI1 molecules is critical in determining current amplitude (reviewed in Fahrner et al., 2018; Yen and Lewis, 2019), whereby the net $Ca^{2+}$ influx is governed by STIM1 and ORAI1, and other SOCE homologs play essential modulatory roles (Hoth and Niemeyer, 2013). Since the identification of STIM and ORAI, the stoichiometries of the ORAI channel, STIM molecules, and the complex between them have been extensively studied (as summarized in recent reviews by Nwokonko et al., 2017; Qiu and Lewis, 2019). Early studies pointed to a homotetrameric stoichiometry of functional channels (Mignen et al., 2008). Other groups also claim that STIM-bound ORAI1 channels form tetramers based on experiments using a range of techniques including Förster resonance energy transfer (Ji et al., 2008; Madl et al., 2010; Maruyama et al., 2009; Penna et al., 2008). STIM-free ORAI1 in the resting state has been reported to be dimeric (Demuro et al., 2011; Penna et al., 2008), suggesting that STIM1 induces multimerization of ORAI1 in the ER–plasma membrane junctions. The finding that ORAI1 is present at dimers at rest has also been suggested in a recent study by Li et al., who also found that the STIM1-dependent multimerization of ORAI1 requires the presence of the cytosolic α-soluble *N*-ethylmaleimide–sensitive factor (NSF) attachment protein (α-SNAP) (Li et al., 2016). However, the view of dimeric and tetrameric ORAI channels has been challenged. The crystal structure of a truncated *Drosophila* ORAI1 has been determined, and revealed a trimer of dimers, proving that the closed and open channel is a hexamer (Hou et al., 2018, 2012). Also, the main conformation of ORAI channels in a constitutively open *Drosophila* ORAI1 mutant (P288L) was found to be hexameric (Liu et al., 2019), and studies using concatenated hexamers proved functionality of the tethered subunits (Cai et al., 2016; Yen et al., 2016). However, it should be noted that the applied crystallography and biochemical methods require extraction of proteins from their native environment, while methods using directly tagged fluorescent proteins lack single-molecule resolution, and the functionality of concatenated constructs might not exclude the existence of dimers. Although these studies contributed considerably to our understanding of the constituents mediating SOCE, we aimed to develop approaches that allow us to monitor proteins in a native environment.

Here, we address the question of whether ORAI1 was present as a homodimer in the intact plasma membranes of HEK cells. Liquid-phase scanning transmission electron microscopy (STEM) (de Jonge and Ross, 2011; Peckys and de Jonge, 2014) was utilized to map the locations of labeled ORAI1 proteins in whole cells in the native liquid state. The samples were protected from drying in the vacuum of the electron microscope by coating with a graphene sheet (Dahmke et al.,

[1]Molecular Biophysics, University of Saarland, Center for Integrative Physiology and Molecular Medicine, 66421 Homburg/Saar, Germany. [2]INM – Leibniz Institute for New Materials, 66123 Saarbrücken, Germany. [3]Department of Physics, University of Saarland, 66123 Saarbrücken, Germany.

*Authors for correspondence (barbara.niemeyer@uks.eu; niels.dejonge@leibniz-inm.de)

N.d.J., 0000-0002-3969-6821

**Received 10 October 2019; Accepted 2 December 2019**

Journal of Cell Science (2020) 133, jcs240358. doi:10.1242/jcs.240358

2017). In our previous study (Peckys et al., 2016), a specific nanoparticle label was developed for the ORAI1 protein via an extracellular HA tag to attach quantum dots (QDs) for visualization with STEM. While this initial study showed the feasibility of labeling ORAI1 proteins in Jurkat T cells by QDs, only sparse labeling was obtained and the results were potentially obscured due to homo- and hetero-multimerization with endogenous untagged ORAI1 or ORAI2 proteins (Jurkat cells express little ORAI3). As a result, the intention of this current work is to further investigate whether ORAI1 channels in intact membranes can form dimers at rest using expression in HEK293 cells. HEK293 cells were selected as they express less endogenous ORAI proteins compared to Jurkat T cells (Alansary et al., 2015). To aid in this, an optimized labeling protocol was developed by enhancing the accessibility of the HA tag through the deletion of the N-glycosylation site. Additionally, two types of QDs were used with different diameters, the smaller QDs showing improved labeling efficiency. Individual label positions were measured from high-resolution STEM data that was obtained. Several ORAI1 constructs were studied involving concatenated (linked) ORAI1 homodimers with either one or two label-binding positions. A statistical analysis was performed to reach a conclusion regarding the presence of homodimers. Experiments were complemented by a biochemical approach involving native gel electrophoresis.

## RESULTS

### HA-tagged ORAI1 mediates a characteristic $I_{CRAC}$

For detection of ORAI1 proteins with STEM, an ORAI1 construct with an extracellular tag was cloned. A small, 9-amino-acid HA tag was used within the second extracellular loop of ORAI1 for labeling the protein with a QD (Gwack et al., 2007; Peckys et al., 2016). The QDs bound via an anti-HA Fab antibody fragment extracellularly added to transfected cells. In the case of ORAI1 existing as a homodimer, correctly QD-labeled subunits would appear as dimers in STEM. To be able to calibrate the amount of expressed protein without adding a large fluorescent tag directly to the protein, GFP–P2A–ORAI1 plasmids were generated. Upon expression, the P2A peptide is cleaved by endogenous proteases (Fig. 1A), resulting in a 1:1 stoichiometry of cytosolic GFP and membrane-delimited ORAI1, which enabled a direct correlation of ORAI1 expression levels with the GFP fluorescence. With fluorescence microscopy, a cytosolic GFP and membrane-delimited HA localization were detected using a Fab fragment directly conjugated to a fluorophore (Fig. 1B). To confirm the functionality of the P2A-linker-cleaved ORAI1 protein, whole-cell currents were recorded from HEK293 cells stably expressing STIM1 proteins (denoted HEKS1 cells) (Soboloff et al., 2006) and transiently transfected with GFP–P2A–ORAI1 or a bicistronic ORAI1–IRES–GFP construct, which is considered a standard control for untagged ORAI1 expression. Both constructs mediated identical current densities with a characteristic current–voltage (*I–V*) relationships and identical amplitudes (Fig. 1C–E), confirming that the post-translational cleavage of ORAI1 from GFP does not alter functionality.

HEK cells were used to examine the localization of single ORAI1 proteins. To the cells, we applied CRISPR/Cas9-mediated gene deletion of endogenous *ORAI1* and *ORAI2* genes (denoted HEK CRI1). These cells showed a significant reduction in $Ca^{2+}$ influx (Fig. S1A) and were then used for acquisition of electron microscopy data.

### Detecting QD-labeled single ORAI subunits by electron microscopy

HEK CRI1 cells were transfected with ORAI–HA constructs, and the expressed ORAI–HA proteins were labeled with QDs. Cells were first fixed with a combination of 3% formaldehyde and 0.2% glutaraldehyde to avoid fixation artifacts, and to achieve a rapid and complete fixation of membrane proteins (Kusumi and Suzuki, 2005; Schmidt et al., 2019). Subsequently, a two-step labeling protocol using an incubation with biotinylated anti-HA Fab was followed by labeling with QD655 (Peckys et al., 2016). Light microscopy images were recorded to identify GFP-expressing and QD-labeled cells, showing that QD fluorescence signals were homogenously

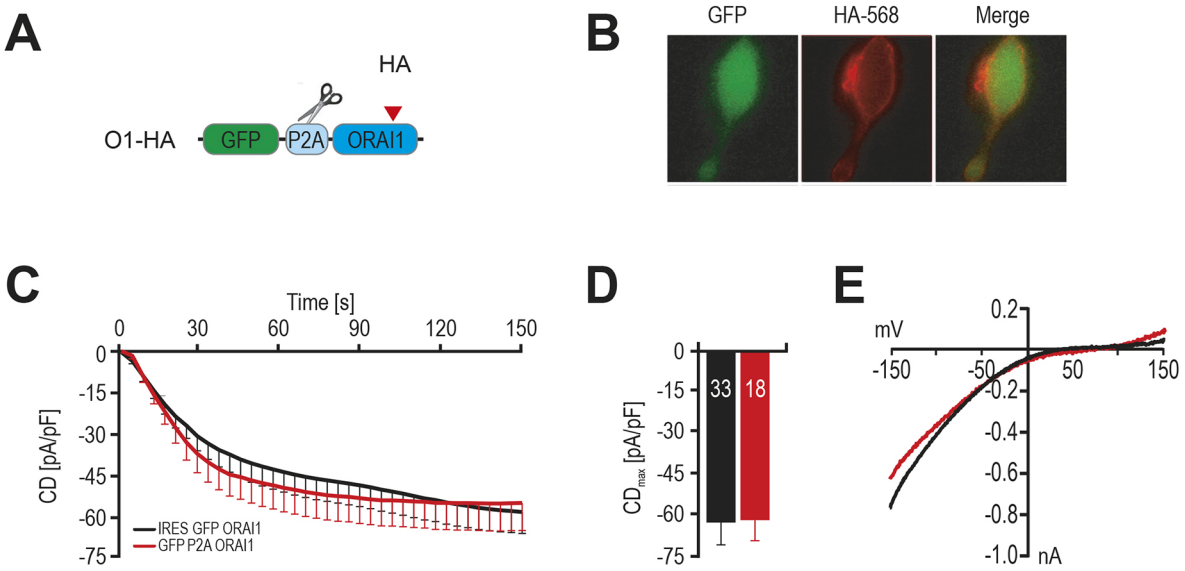


**Fig. 1. Characterization of functional HA-tagged ORAI1 constructs.** (A) Schematic representation of the GFP–P2A–ORAI1 construct for stoichiometric expression of GFP and an extracellular HA tag. (B) Fluorescent signals obtained from HEK CRI1 cells transfected with the construct shown in (A) and stained with a fluorophore-conjugated anti-HA antibody without permeabilization (HA-568, red) and the cytosolic signal of the GFP (green). (C) Average (mean±s.e.m.) traces showing whole-cell current density (CD) over time extracted at −130 mV in HEKS1 cells transfected with 1 µg ORAI1–IRES–GFP (black trace) or 1 µg GFP–P2A–ORAI1 (red trace). (D) Maximum CD (mean±s.e.m.) recorded from cells measured in C; *n* values are given in the column. (E) Corresponding current–voltage (*I–V*) relationship of representative cells recorded in C.

Journal of Cell Science (2020) 133, jcs240358. doi:10.1242/jcs.240358

dispersed over the plasma membrane, as would be expected for ORAI1 localization in non-activated cells (data not shown). A second fixation step with 2% glutaraldehyde was then performed to provide sufficient stability during electron beam irradiation. Afterwards, the samples were coated with multilayer graphene to preserve the hydrated state within the vacuum chamber of the electron microscope (Dahmke et al., 2017). Whole cells were examined using STEM. An example of a typical high-resolution STEM image is shown in Fig. 2A, with detected QDs outlined in yellow. This STEM image revealed a surface density of 90 QDs/$\mu m^2$, compared to 3 QD labels/$\mu m^2$ for untransfected cells in a control of the labeling specificity (see Table 1). While many QDs appear to exist in pairs, possibly indicating the presence of ORAI1 dimers, many single QD and some larger groups are also apparent. Likely, not all existing ORAI1 positions were labeled due to limited labeling efficiency. Aiming for a close as possible mapping of ORAI1 positions with QDs, the labeling protocol was changed to increase the labeling efficiency.

### The use of smaller QDs and prevention of N-linked glycosylation improved accessibility of labels

To increase the labeling efficiency, a series of experiments was performed. It is reasonable to assume that the HA tag position (tag inserted after R210) near a large extracellular sugar moiety (attached to N223) might hinder QD binding (Fig. 3A). First, a N223A mutation was introduced into the tagged ORAI1–HA protein, thus removing the extracellular sugar moiety (Fig. 3B) (Dörr et al., 2016). To control for equal functionality, we measured SOCE and the $Ca^{2+}$ release activated current ($I_{CRAC}$) in cells stably expressing STIM1 (HEKS1 cells) and transiently transfected with the generated ORAI1-N223A–HA mutant to be compared to wild-type (WT) constructs. Fig. 3B–G (see black and red traces and bar graphs for the monomer traces) shows that the introduction of N223A did not significantly alter SOCE in HEKS1 cells. Thus, the addition of complex glycans to the ORAI protein had no effect on the current densities.

To rule out misinterpretations of the electron microscopic data due to a possible presence of pre-clustered QDs (QD aggregates that had formed independently of protein binding), control experiments were conducted including tests for self-aggregation of QDs, multiple QDs binding at a single Fab, and unspecific background due to QDs binding at non-HA tag epitope cell-free biotinylated microchips. Results of the test series confirmed the absence of pre-clustering, thus our labeling approach did not exceed a probe to protein ratio of 1:1 (see Fig. S2 and Table S1) as desired. The next measurement obtained was the label density of HA-bound QDs on the surface of cells expressing ORAI1 N223A using STEM; it was found that the label density of detected QDs increased by 74% (see Table 1). To further improve the relative labeling efficiency, the smallest available streptavidin-conjugated QDs were used, since it is known that the labeling efficiency rises with decreasing label size (Howarth et al., 2008; Robinson et al., 2000). It should be noted that the STEM images only show the electron-dense core of the QDs, not their shell or the conjugated streptavidins. Images were taken of negatively stained samples with immobilized QD565 or QD655 to determine the overall size. These samples revealed a core diameter of 5 nm and a total diameter 12 nm for the spherical QD565, and a core size of 7×12 nm and total dimensions of 14×18 nm for the bullet-shaped QD656 (Fig. S3).

A new series of experiments was performed, applying the same protocol as described above for expression and labeling of ORAI1 N223A, except replacing QD655 with the smaller QD565. Fig. 2B shows an example in which ORAI1-N223A–HA-expressing HEK CRI1 cells were identified by their co-expressed GFP (green) and by their QD (red) fluorescence signals. The same region of interest was identified in an overview STEM image (Fig. 2C). A series of high-resolution STEM images was then acquired from the selected cells showing the QD labels with a typical example shown in Fig. 2D. Selected cells expressing ORAI1-N223A–HA within the full range of ORAI1 membrane expression levels, levels being low, medium, and high expression, were selected and imaged with STEM at high resolution. Measuring label densities with the smaller

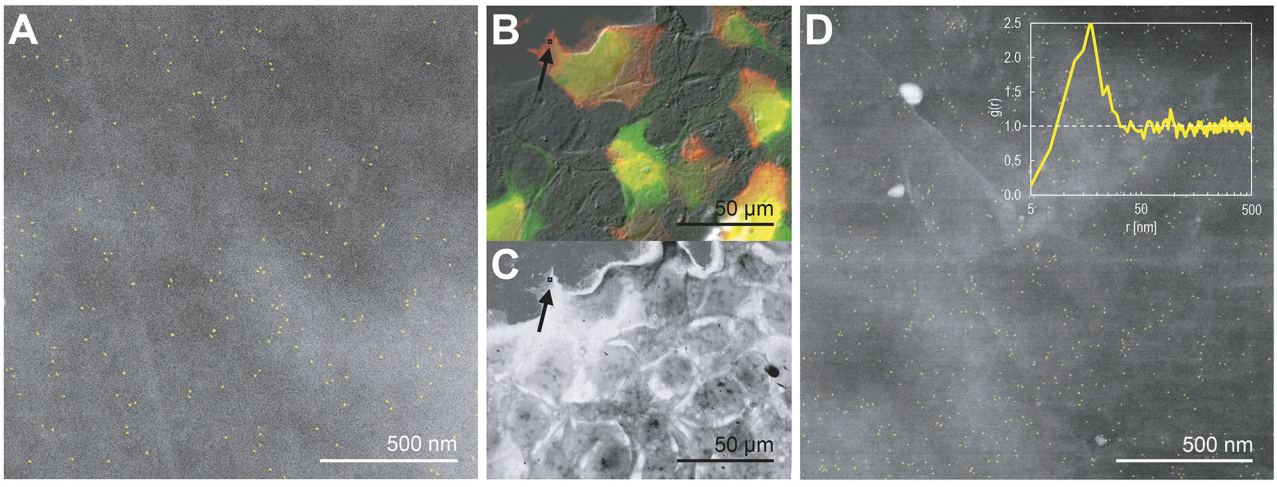


**Fig. 2. Correlative light and electron microscopic images of QD-labeled ORAI1–HA in HEK CRI1 cells.** (A) ORAI1–HA labeled with QD655. Detail from a high-resolution STEM image (120,000× magnification) showing bright QD labels on a dark cellular background, with faint shadows of folds in the covering graphene layer. The image was automatically processed to detect QDs (outlined in yellow). (B) ORAI1-N223A–HA labeled with QD656. Differential interference contrast (DIC) and fluorescence overlay image of a region from the window area of a microchip with adherently grown, transfected and QD-labeled cells. Cells expressing ORAI1–HA light up in green, showing the corresponding reporter GFP expression, and in red, displaying the signal captured in the QD565 fluorescence channel. The QD signal is equally dispersed throughout the plasma membrane, indicating homogenous ORAI1 distribution. (C) STEM image recorded in low-magnification mode (1000× magnification) from the same region shown in B, allowing to the location of ORAI1–HA-expressing cells. (D) Detail from a high-resolution STEM image (120,000× magnification) showing detected QDs in yellow. The image was recorded at the position of the arrows in B,C. The pair correlation function $g(r)$ of all detected QD labels in this image is shown in the upper right corner of the image.

Journal of Cell Science (2020) 133, jcs240358. doi:10.1242/jcs.240358

**Table 1. Data of ORAI1-labeling experiments performed in HEK CRI1 cells**

| Expressed ORAI1 | QD | Number of cells | Number of labels | Label density/μm$^2$ | Analyzed area (μm$^2$) |
|---|---|---|---|---|---|
| Non-transfected | 565 | 4 | 35 | 3 | 12 |
| ORAI–HA | 655 | 13 | 58,324 | 90 | 645 |
| ORAI-N223A–HA | 655 | 12 | 157,729 | 157 | 1007 |
| ORAI-N223A–HA | 565 | 11 | 76,126 | 304 | 251 |
| ORAI N223A concatemer with 1 HA tag at subunit 1 [(O1–HA)–O1] | 565 | 7 | 21,116 | 112 | 188 |
| ORAI N223A concatemer with 1 HA tag at subunit 2 [O1–(O1–HA)] | 565 | 7 | 22,664 | 149 | 152 |
| ORAI N223A concatemer with 2 HA tags [(O1–HA)–(O1–HA)] | 565 | 8 | 42,420 | 270 | 157 |

Different constructs were studied: one expressing ORAI1–HA, and three different types of dimeric ORAI–HA concatemers; one carrying two HA tags; and two with only one ORAI1–HA tag, at the first or at the second ORAI1 subunit. The information includes the number of examined cells, the number of detected QD labels, the average label density, and the total analyzed membrane area.

QD565 revealed an almost doubling of the surface density of detected labels. Additionally, there was an overall increase in label surface density, together with the N223A mutation, as compared to glycosylated ORAI1 tagged with the larger QDs, by 240%.

Fig. 2D shows a complex pattern of the QD labels in which monodispersed QDs can be distinguished as well as pairs of labels and larger clusters, occasionally arranged linearly. The interpretation of this image is not straight forward. Despite achieving an increased labeling efficiency, 100% labeling efficiency was probably not obtained due to the limited binding strength of Fab to HA. In addition, the combined Fab and QD linker exhibited structural flexibility such that the distance between a pair of QDs attached to an ORAI1 dimer had a range of several tens of nanometers. Thus, a direct visualization of the stoichiometric assembly of the ORAI1 $Ca^{2+}$ channel was probably impossible. To further investigate whether labeled ORAI1 proteins were present, preferably as pairs, a statistical analysis of label positions was performed as described in the following section.

### Statistical analysis via the pair correlation function

From all STEM images, the positions of the QDs were automatically determined and analyzed for the presence of ORAI1 dimers. A difficulty in the analysis of label positions is the uncertainty of whether two nearby labels were coupled to a dimer or if the labels were randomly positioned at that distance. For this reason, a statistical analysis was performed using the pair correlation function $g(r)$. For a purely random distribution of labels, one would expect there to be no preferred distance between the labels, and that one would not measure distances smaller than the diameter of the label. The $g(r)$ measures the probability of a certain pair distance to occur using a mathematical function in a radial symmetry (Stoyan and Stoyan, 1996). Labels in a random distribution would yield $g(r)=1$. However, if a certain label distance $x$ would be preferred, for example, by the binding of two labels to a dimer, one would measure $g(r)>1$.

The $g(r)$ measuring center-to-center pair distances of the individual QD565 labels detected in the image shown in Fig. 2D is shown in the inset. Starting at low $r$, $g(r)$ rises from zero upward reflecting the finite size of the QDs consisting of a hard core of 5 nm with a soft shell of 7 nm (see above and Fig. S3). For distances 10–30 nm $g(r)>1$, a peak is present at $r=18$ nm. The function tends towards $g(r)=1$ for $r>30$ nm, indicating a random distribution of labels spaced further apart. Note that the peak height of $g(r)$ measures the abundance of pairs relative to the label surface density, with lower densities resulting in higher absolute peak values. An analysis of the control experiment using samples with randomly positioned QDs chemically immobilized directly on the silicon nitride (SiN) membrane, thus without cells, confirmed $g(r)=1$ for $r$ larger than the diameter of core and shell of the nanoparticle, and the absence of any peak (Fig. S2).

The observed higher than random probability of QD center-to-center distance of 18 nm is consistent with a schematic molecular model of ORAI1 protein oligomers with attached labels (Fig. 4A). From this, the range of distances expected to span QD labels and their positioning at the ORAI1-N223A–HA subunits in multimeric conformations was estimated. The established model predicts center-to-center distances of two QDs labeling two subunits of an ORAI–HA dimer of 10 to 30 nm. The finding that QD labels are present in pairs shows that ORAI1 proteins were present in oligomers, that is homodimers or higher-order oligomers to which two QDs had bound. However, our data does not allow us to draw a conclusion about the stoichiometry of the oligomer. For example, pairs of labels or more than two labels could also be bound to ORAI1 hexamers yielding a very similar pair distance range as for homodimers (Fig. 4B). Note that for $r=50$–$500$ nm, $g(r)$ values slightly above 1 could possibly indicate a minor degree of ORAI clustering at a scale larger than protein oligomers; however, it is more likely that this effect is due to bends in wrinkled membrane areas leading to slight deviations from a completely horizontal orientation, for instance at the cell edges. This may result in a shortening of distances from the imaging top perspective.

### Analysis of concatenated ORAI1 dimers

In order to investigate the presence of ORAI1 homodimers or higher-order oligomers, further experiments were conducted by generating three additional ORAI1 constructs in an N223A background. Herein, GFP–P2A concatenated dimeric ORAI1 constructs were generated, which either included the extracellular HA tag in both subunits of the dimer [(HA–O1)–(O1–HA)] or alternatively only in the first [(HA–O1)–O1] or the second subunit [O1–(O1–HA)] (Fig. 5A). Fluorescent microscopy was used to correlate GFP expression with the signal strength obtained by immunolabeling of the HA tag. As described previously, an Alexa-Fluor-586-tagged Fab fragment of an anti-HA antibody was used to ensure a 1:1 label. Fig. 5B,C shows that fluorescent signals detected in HEK CRI1 cells transfected with the concatenated double-tagged dimer were indeed twice as high as those obtained with the single-tagged ORAI1 dimer or with the monomer (Fig. 5B,C). In preparation for STEM imaging, the relative labeling efficiency was deduced from the amount of bound fluorescent QDs in comparison to expression levels. Plotting the single-cell values for constructs expressed in HEK CRI1 cells for average GFP and QD fluorescence intensities showed a linear correlation between both fluorescence signals, from which linear regression lines were

Journal of Cell Science (2020) 133, jcs240358. doi:10.1242/jcs.240358

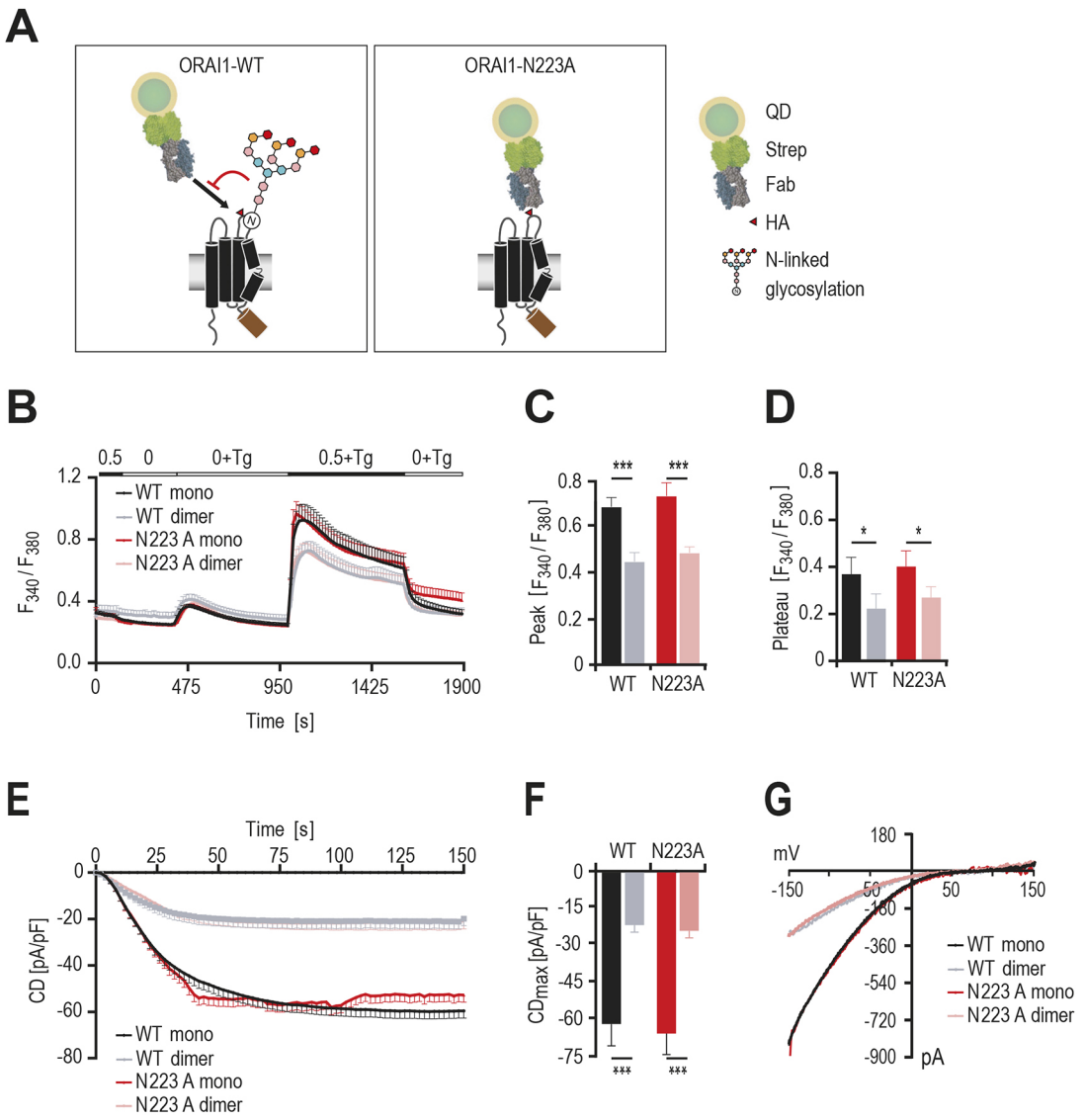


**Fig. 3. Characterization of ORAI1 constructs with optimized HA accessibility.** (A) Schematic representation of accessibility of the HA epitope to the Fab fragment and the coupled streptavidin-QD in ORAI1-WT (left panel) showing potential steric hindrance by the attached sugar moiety compared to the glycosylation-deficient mutant ORAI1-N223A (right panel). (B) Changes of the fluorescence ratio of fura-2 reflecting changes in intracellular $Ca^{2+}$ concentrations over time upon store depletion and $Ca^{2+}$ re-addition induced by solution exchange as shown on the bar above the traces. Measurements were performed in HEKS1 cells transfected with ORAI1-WT monomeric (black trace) or dimeric (gray trace) constructs compared to the ORAI1-N223A monomeric (red trace) or dimeric (rose trace) constructs (black trace, *n*=73; gray trace, *n*=65; red trace, *n*=33; rose trace, *n*=51). (C) Quantification of the maximum change in fluorescence ratio and (D) steady state fluorescence of cells measured in (B) with the same color code. (E) Average traces showing whole-cell current density (CD) over time extracted at −130 mV in HEKS1 transfected as in B. (F) Maximum CD and (G) representative *I*–*V* relationships of currents measured in E. Results are shown as mean±s.e.m.; *n*=11–30.

calculated (Fig. 5D). The calculated regression lines of their GFP to QD intensity correlation had slopes of 1.02 for the (HA–O1)–(O1–HA) double-tagged dimer, versus 0.43 and 0.39 for the O1–(O1–HA) and (HA–O1)–O1 single-tagged dimers. The corresponding $R^2$ values were 0.35, 0.52 and 0.65, respectively. Compared to the double HA-tagged dimer, both single HA-tagged dimers showed a ∼50% reduction of the slope. Therefore, it can be concluded that all three dimer constructs had a similar labeling efficiency per HA tag.

To confirm functionality of the concatenated dimers, $Ca^{2+}$ imaging and patch-clamp experiments in HEKS1 cells were performed. These revealed that concatenated dimers show decreased function compared to an expressed monomer, though this effect is independent of the presence or absence of N-linked glycosylation (Fig. 3B–G).

### Examining the presence of ORAI1 homodimers

STEM was performed after expression of the three different ORAI1 dimeric concatemers in HEK CRI1 cells to address the question of whether ORAI1 was present as a dimer or higher order oligomers, with exemplary images shown in Fig. 6A-C. Remarkably, all images showed clusters of labels as well as single labels. This result was confirmed by the *g*(*r*) analysis of all STEM images of the four groups, shown in Fig. 6D (see also Table 1). The three *g*(*r*) graphs of the concatemer experiments each exhibited a similar spatial peak profile as the monomeric ORAI1-N223A-HA protein, whereby the maximum of the single HA-tagged concatemers were about 2 times higher than the double-tagged concatemer. This outcome is expected due to the ∼50% lower density of labels in cells expressing the single HA-tagged concatemers. The important conclusion of this *g*(*r*)

Journal of Cell Science (2020) 133, jcs240358. doi:10.1242/jcs.240358

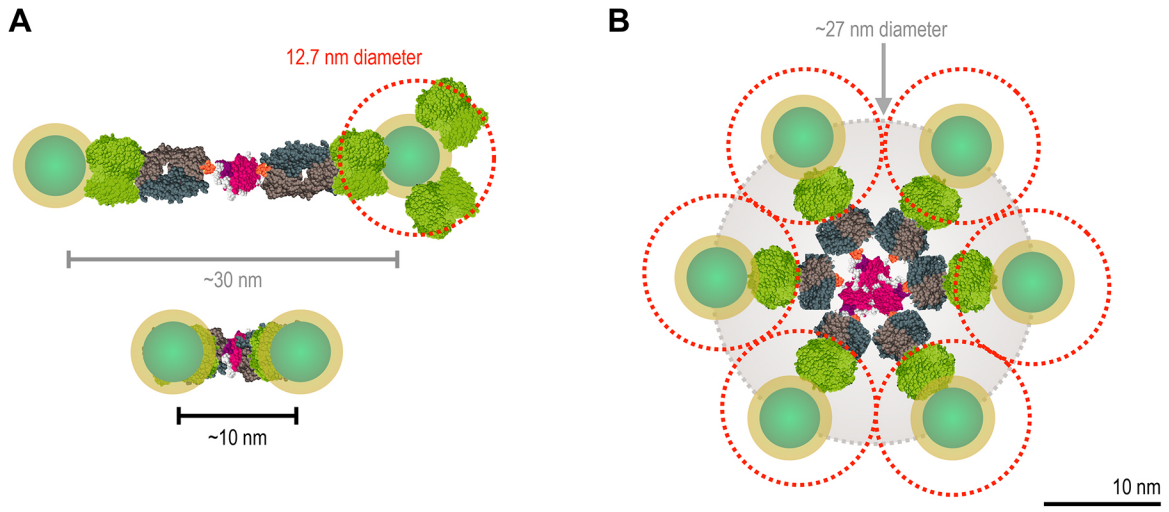


**Fig. 4. Theoretical models depicting the possibilities of QD-labeling ORAI1 in dimer or hexamer configuration.** (A) Top view of membrane-anchored ORAI1 dimer (pink); each subunit has a HA tag (orange) on the extracellular side. Anti-HA biotinylated Fab (brown/gray) can bind to the HA tags, each providing a binding position for a streptavidin (green)-conjugated quantum dot (QD565), shown with their electron-dense QD core (green), and electron-transparent shell (yellow). With this labeling approach, the maximum QD:ORAI1 ratio is 1. Bound QDs can be flexibly positioned; for instance, they can horizontally stretched out, as shown in the upper configuration, reaching a QD center-to-center distance up to ~35 nm (gray line), or more upright (lower configuration), coming as close as ~10 nm (black line). A dotted red circle indicates the average QD565 diameter of 12.7 nm (as measured from TEM images of negatively stained QD565, see Fig. S3), including a few conjugated streptavidin molecules per QD (for convenience, most QDs are drawn with only one streptavidin). (B) Top view of a hexameric ORAI1 oligomer maximally labeled with QDs. This configuration would be expected to yield circular label symmetry with a maximum diameter of upright standing labels of ~27 nm. Relative sizes and shapes of the protein structures are derived from the Protein Data Base (surface rendering in JSmol; streptavidin: 4YVB; anti-HA Fab–biotin represented by: 4YVB, one Fab fragment without biotin; HA tag: schematic small protein; ORAI1 dimer: 4HKR, asymmetric unit).

analysis is that dimers with only one HA tag also assembled in pairs. A conclusion can now be drawn on the stoichiometry of ORAI1. Since concatenated dimers with only one possible QD-binding position assembled in pairs, it follows that ORAI1 at rest must have been present in larger oligomers than dimers, possibly tetramers or hexamers. If they had remained as individual dimers in the membrane, the single HA tag position would have shown a random label distribution without a peak.

## Biochemical approach

In parallel to the microscopy, one goal was to validate the ORAI1 stoichiometry using biochemical approaches. First, either membrane

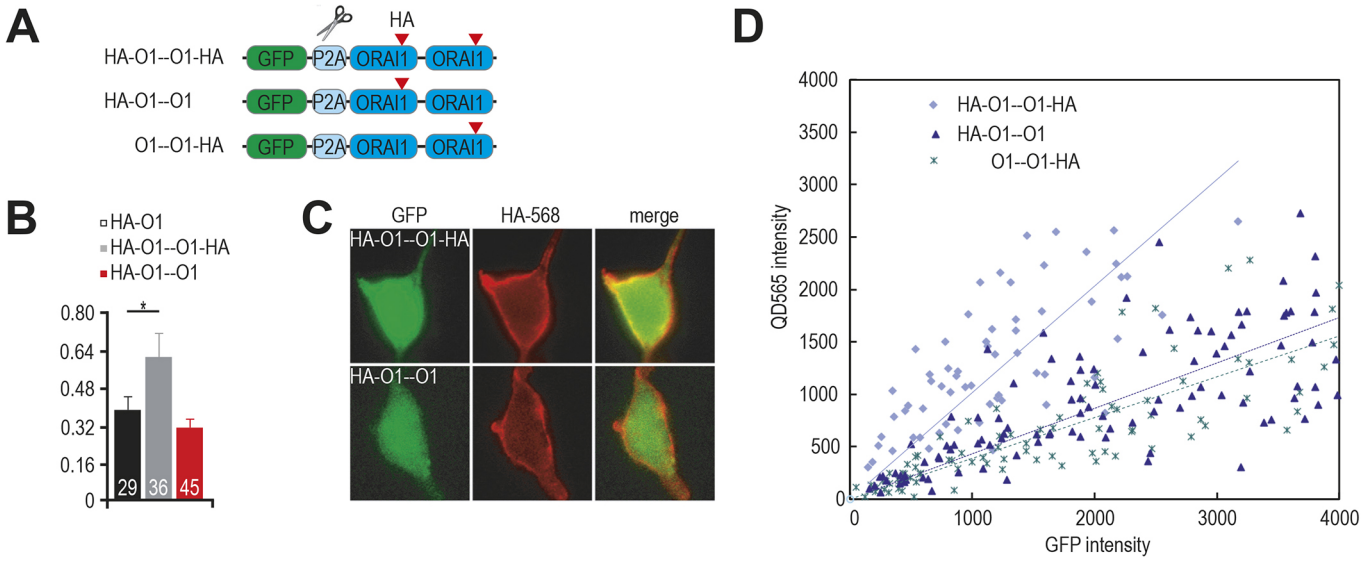


**Fig. 5. Labeling of different concatenated dimeric ORAI1 constructs.** (A) Schematic representation of the concatenated dimeric ORAI1 constructs showing the cleavable P2A peptide and the position of the HA tag in one or both subunits of the dimeric construct. (B) Quantification (mean±s.e.m.) of the plasma membrane signal of the monomeric (black bar showing the average of cells represented in Fig. 1B) and dimeric constructs (gray bar for HA-O1–O1 HA and red bar for HA-O1–O1) normalized to the cytosolic GFP signal; *n* values are given in the column. (C) Fluorescent signals obtained from HEK CRI1 cells transfected with the double tagged ORAI1 (HA-O1–O1-HA, upper row) or with the single tagged ORAI1 construct (HA-O1–O1, lower row) and stained with a fluorophore coupled anti-HA antibody without permeabilization (HA-568, red) and the cytosolic signal of the GFP (green). (D) Corresponding analysis for the three dimeric concatemers of ORAI1–HA, expressed in HEK CRI1 cells. The two single ORAI1 HA-tagged dimers HA-O1–O1 (filled dark blue triangles), and O1–O1-HA (dark green crosses) show a ~50% lower slope of their GFP/QD intensity correlation than the double HA-tagged HA-O1–O1-HA dimer (filled bright blue diamonds), because they offer only half of the binding positions for the labels.

Journal of Cell Science (2020) 133, jcs240358. doi:10.1242/jcs.240358

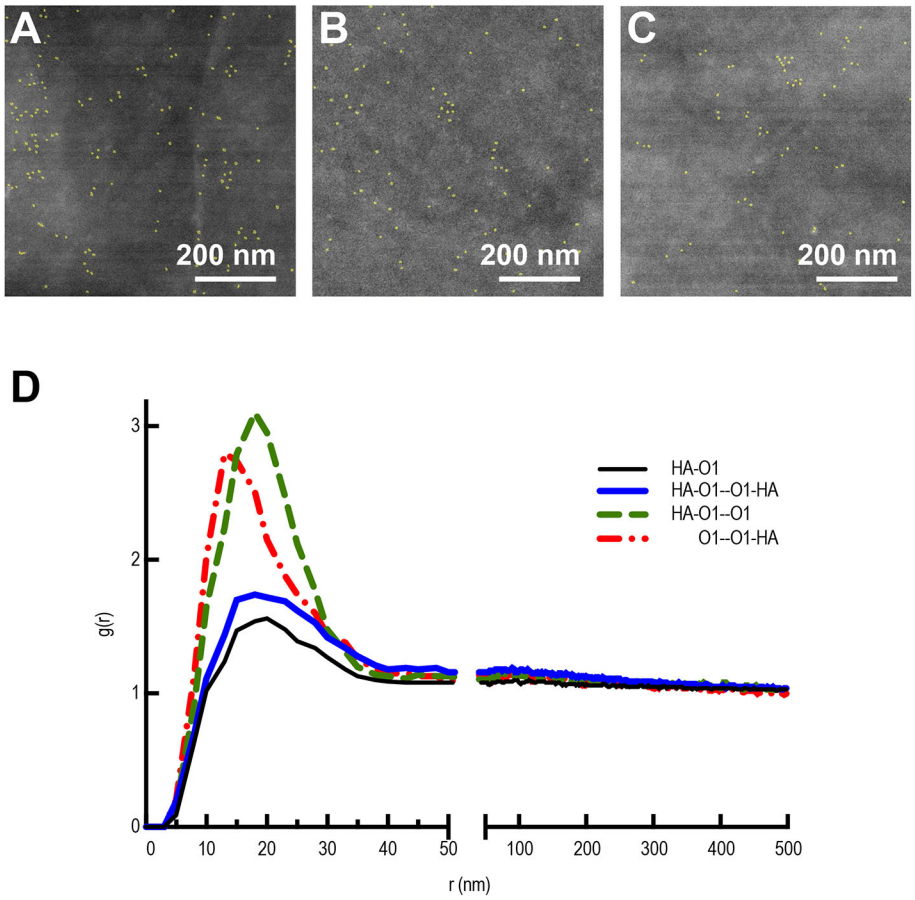


**Fig. 6. STEM images of concatenated ORAI1.** STEM images recorded in high-magnification mode (120,000× magnification) from QD565-labeled cells expressing the dimeric ORAI1 concatemers. (A) Dimeric concatemer with both subunits HA-tagged (HA-O1–O1-HA), (B) concatemer with one HA tag at the first subunit (HA-O1–O1), or (C) at the second subunit (O1–O1-HA). In all three images, labels are found clustered, demonstrating that concatemeric ORAI1 assembles in oligomers of ≥4. (D) Pair correlation function $g(r)$ of QD-labeled ORAI1–HA and its dimeric concatemers. The $g(r)$ function of the pooled data of ORAI1–HA (11 cells, $n$=76,126 detected QDs) shows a prominent peak from ≥10 to 30 nm, and a maximum between 17.5 and 20 nm. The three different ORAI1–HA concatemers [HA-O1–O1-HA (42,420 labels), HA-O1-O1 (21,116 labels), and O1–O1-HA (22,664 labels)] yield $g(r)$ results with peaks of similar widths and maximum positions at 17.5 nm, whereby O1–O1-HA has its maximum shifted towards 12.5 nm. The ∼2-fold higher peak values for the single HA-tagged concatemers, compared with the dimer having two HA-tags (and also with the ORAI-HA wild-type variant), are a result of the∼50% lower label density in experiments with these concatemers.

permeable (DSP) or impermeable (BS3) chemical cross-linking reagents were applied to intact cells stably expressing ORAI1 N223A (denoted HEK N223A), then the obtained molecular masses were analyzed by non-reducing SDS gel electrophoresis. Lane profile analysis showed that a major fraction of ORAI1 proteins existed as monomers (42%) and dimers (27%) followed by tetramers, representing ∼20% of the total protein, while hexamers existed as only ∼10% of the total protein (see Fig. 7A,B). To concentrate potential oligomers in the plasma membrane fraction and to exclude possible dilution with monomers included in the whole-cell lysate, and to address the question of whether the ORAI1 oligomers assembled intracellularly or at the plasma membrane, we combined cell surface biotinylation with cross-linking experiments. For this the non-permanent cross-linker was used after labeling surface membrane proteins with biotin and consequently isolating membrane fraction using avidin beads. A combination of cell surface biotinylation and cross-linking approaches showed that the fraction of higher molecular weight multimers of ORAI1 at the plasma membrane (Fig. 7C,D) was not different from that found in the whole lysate (Fig. 7B), which agrees with the results obtained with the membrane permeable cross-linker DSP and suggests that ORAI1 is not assembled at the plasma membrane.

Because the fraction of monomeric proteins in the cross-linking experiments was surprisingly high compared to the crystal structure data indicating a hexameric ORAI stoichiometry (Hou et al., 2012; Liu et al., 2019), it is reasonable that this high fraction may have been due to either a limited efficiency, binding affinity or spacer length, of the cross-linker or to sensitivity of the formed complexes to SDS. Therefore, ORAI1 protein complexes were resolved by molecular weight, while retaining their native structure in very mild solubilization conditions using Blue Native PAGE (BN-PAGE) of HEK N223A cells. Exact determination of the molecular mass of the detected complex was hampered by the dependence of the separation pattern not only on the molecular mass, as is the case in denaturing gels, but also on potential associations with interacting partners, and on the lipid composition of the protein milieu. Using two different protein markers, the Blue Native gel analysis revealed that only one significant higher molecular mass complex was detected upon expression of the monomeric ORAI1 (Fig. 7E). These results indicate that ORAI1 forms a single high molecular mass complex with an apparent molecular mass between 232 and 440 kDa, indicating, within the error margin of the method, a configuration larger than a dimer.

As the HEK CRI1 cells still showed a residual $Ca^{2+}$ response and as the *ORAI3* gene was not targeted, a second CRISPR cell line was initiated with gene deletion of all endogenous *ORAI1-ORAI3* genes (HEK CRI2, see Fig. S1). Sequencing of genomic DNA extracted from monoclonal cell lines identified different nucleotide deletions within the coding regions of *ORAI1, ORAI2* and *ORAI3* (Fig. S1B), resulting in frame shift mutations in all three proteins. For ORAI1, the absence of protein was confirmed by western blotting (Fig. S1C); for ORAI2 and ORAI3, the concentrations of HEK cell endogenous ORAI2 or ORAI3 proteins were too low to detect with several tested commercial antibodies. However, absence of functional proteins was confirmed by genomic sequencing, as well as the complete abolishment of SOCE (Fig. S1D). In the STEM analysis, we confirmed that despite the presence of residual ORAI proteins in CRI1 cells, no significant differences were detected in the pair correlation function after overexpression of ORAI1 when compared to overexpression in HEK CRI2 cells (Fig. S4). In

Journal of Cell Science (2020) 133, jcs240358. doi:10.1242/jcs.240358

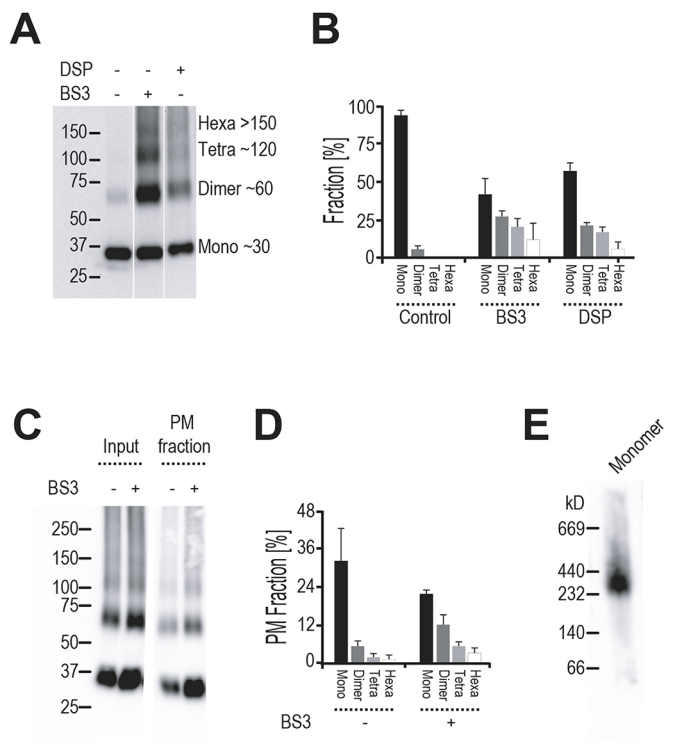


**Fig. 7. Biochemical analysis of ORAI1 stoichiometry.** (A) Representative western blot showing monomeric and multimeric fractions of ORAI1 in cells treated with membrane impermeable (BS3) or permeable (DSP) cross-linker. Experiments were performed in HEK293 cells stably expressing HA-tagged glycosylation-deficient ORAI1 (HEKO1 N223A). (B) Quantification (mean ±s.e.m.) of the monomeric or multimeric fractions obtained from six independent experiments and analyzed by Igor software using the multi-peak profile plug-in. (C) Representative western blot showing the stoichiometry of ORAI1 at the plasma membrane. Resting HEKO1 N223A cells were subjected to BS3-mediated cross-linking followed by surface protein biotinylation. Biotinylated fractions were extracted with avidin beads and quantified (D) (mean±s.e.m., $n$=6) as fractions of the total proteins measured from total cell lysates (input). (E) Representative western blot of a Blue Native PAGE showing ORAI1 obtained from lysates of resting HEKO1 N223A cells, showing that ORAI1 exists mainly as a single complex of an estimated molecular mass higher than calculated for a dimeric channel.

addition, Blue Native PAGE analysis expressing the concatenated dimer in a HEK CRI2 background showed the same higher-order molecular mass complex as found in the stably expressed monomer (Fig. S5), also indicating the presence of only one type of high molecular mass complex at rest.

## DISCUSSION

This study applied a novel technique to address the debated question of whether ORAI1 channels exist as dimers at rest within the plasma membrane of intact cells. When combining measurements obtained for different concatenated ORAI1 constructs, our data is inconsistent with the dimer-at-rest model. Instead, our results are consistent with the evidence that ORAI1 is present in hexameric form as found in crystal structures of *Drosophila* Orai (Hou et al., 2018, 2012; Liu et al., 2019). Since experiments with crystal structures used protein crystals obtained from proteins extracted from the plasma membrane, it is important not to rely solely on crystal structures; these proteins underwent solubilization and reconstitution in artificial conditions. The stoichiometry visible in a crystal structure does not necessarily reflect the natural state in the cell, since the crystallization procedure may very well drive the protein complex to crystallize in one particular state under optimized chemical conditions. For example, recent data show that the stoichiometry in the published crystal structure differs from the functional protein in its plasma membrane environment for the class A G-protein-coupled receptors, and moreover revealed the parallel existence of several different oligomeric stoichiometries (Gurevich and Gurevich, 2018).

On the other hand, studies keeping the protein in the cells sometimes lead to different outcomes. For example, a study using GFP photobleaching proposed ORAI1 at rest to exist as dimers (Demuro et al., 2011; Penna et al., 2008), as tetramers (Ji et al., 2008) or as mixed species, which then assemble upon demand (Li et al., 2016). The disadvantage of optical techniques is their insufficient spatial resolution for directly studying stoichiometry (see discussion elsewhere; Peckys et al., 2015). In addition, the photo-bleaching studies rely on fusions of ORAI1 with fluorescent proteins that almost double the molecular mass of ORAI1 and may be affected by dimerization of the added GFP with itself. Furthermore, high laser intensities required for photobleaching likely produce significant amounts of reactive oxygen species. This may decrease the ability of ORAI1 subunits to interact with each other (Alansary et al., 2016), and thus possibly break apart complexes or alter dynamics of *de novo* complex formation. Theoretical models that assumed an assembly-upon-demand and graded activation of ORAI1 by STIM1 were able to fit experimental data (Alansary et al., 2016; Kilch et al., 2013), but also relied on several free parameters. Potentially, the graded activation achieved by different STIM1:ORAI1 binding ratios may be the sole underlying principle to explain activation (Yen and Lewis, 2019). A new experimental option to study membrane proteins is provided by whole-cell electron microscopy in liquid (De Jonge, 2018). For example, Maruyama et al. used a related atmospheric scanning electron microscopy to detect dynamic string-like assemblies of STIM1 within the ER of activated cells (Maruyama et al., 2012).

Our study now adds evidence to this debate by showing that the higher-order oligomers exist for ORAI1 at rest in the intact plasma membrane. The interpretation of the $g(r)$ curves requires some consideration. If it is assumed that ORAI1 at rest is present as a hexamer, then the question is how many QD labels would be able to bind. The schematic hexamer molecular model (Fig. 4B) shows that it is possible, in principle, to bind six QD labels. For a predicted center-to-center distance of ∼35 nm, the labels must assemble into an open extended conformation with labels being closest to the plasma membrane, whereas ∼27 nm is predicted for a tightly packed hexagonal conformation where the labels project away from the plasma membrane. However, the STEM data (Fig. 6) does not show clusters of six labels only, but rather a range of sizes and arrangements, whereby most labels reside in clusters smaller than six. This lack of hexameric label clusters is presumably caused by a limited labeling efficiency ($\eta$). The probability to observe six bound labels is equivalent to $\eta^6$, such that for an exemplary value of $\eta$=50%, only 1.6% of the actual hexamers would show up as clusters of six labels. For the STEM method to directly observe hexamers, a different labeling strategy would be necessary to push $\eta$ above a value of ∼90%, so that at least half of the hexamers would be visible as such. A further complication is that the size of one label plus linker, ∼7 nm, is already larger than the hexamer itself (Hou et al., 2011, 2012), so that even with $\eta$=90%, labels from adjacent hexamers would probably overlap. Labeling with nanogold and a small linker might improve the labeling; however, current label efficiencies for nanogold labels are far too low for this to be printable. Moreover, increasing $\eta$ would probably require a different tag than HA. Another possibility is that the overexpressed ORAI1

Journal of Cell Science (2020) 133, jcs240358. doi:10.1242/jcs.240358

complex was mixed with remaining endogenous ORAI. This possibility was ruled out from an additional cell line lacking all three endogenous *ORAI* genes and in which SOCE was completely abolished (Fig. S1B–D). Analysis of label distribution in this cell line neither changed the shape of $g(r)$ (Fig. S4) nor increased the label density (Table S1).

A further question was whether different label binding positions would exhibit different values of $\eta$. The finding that both the first and the second position of the single-tagged concatenated dimer led to similar label surface densities indicates that both positions were labeled with similar labeling efficiencies. Moreover, the second subunit of the concatenated dimer must have been present in a folded form at the surface. Additionally, the amount of QDs attached to a concatenated dimer with two HA tags doubled compared to that of a concatenated dimer with one tag (Fig. 5). Note that a reduction in $Ca^{2+}$ entry and in current density was observed when comparing dimer with monomer (Fig. 3). As both subunits seemed to have folded and were labeled by the anti-HA antibody, reduced function was most likely due to a reduced gating of the tethered subunits; in an earlier study using concatenated hexamers, normalization of current data might have obscured this effect (Yen et al., 2016).

Since label densities doubled for double-tagged concatenated dimers, but no significant differences in the $g(r)$ were observed, we conclude that most detected ORAI1 pairs were predominantly assembled in higher-order oligomers, likely hexamers but possibly also a mixture with tetramers, showing a high probability of binding least 2 QDs. This interpretation of the data is also consistent with the blue native gel analysis showing the presence of one large molecular weight complex of an apparent molecular mass larger than a dimer.

## MATERIALS AND METHODS

### Materials

HEK293 cells were obtained from ATCC (these were regularly tested for the absence mycoplasma). Fetal bovine serum, 2-mercaptoethanol, thapsigargin, cyclopiazonic acid (CPA), and sodium azide, were either from Thermo Fisher Scientific or Sigma-Aldrich. ScreenFect®A transfection reagent was from Incella, Eggenstein-Leopoldshafen, Germany. Anti-HA-Biotin, High Affinity (3F10) from rat IgG1 was from Roche Diagnostics, Mannheim, Germany. Dulbecco's phosphate-buffered saline (DPBS), Dulbecco's modified Eagle's medium GlutaMAX™ with high glucose and pyruvate (DMEM), normal goat serum (GS), CellStripper and Quantum Dot (QD) Qdot® 655 and 565 streptavidin conjugates (strep-QD) were from Thermo Fisher Scientific. ROTISOLV® HPLC grade deionized water, acetone and ethanol, 10× solution phosphate-buffered saline (PBS), 25% solution electron microscopy grade glutaraldehyde (GA), D-saccharose, sodium chloride, glycine, biotin-free molecular biology grade albumin fraction V (BSA), and sodium cacodylate trihydrate were from Carl Roth. Electron microscopy grade formaldehyde (16% solution) was from Science Services, Munich, Germany. 0.01% poly-L-lysine (PLL) solution (mol. mass 70,000-150,000 Da), sodium tetraborate and boric acid were from Sigma-Aldrich. CELLVIEW cell culture dishes (35 mm) with four compartments and glass bottoms were from Greiner Bio-One, Frickenhausen, Germany. Custom-designed silicon microchips were purchased from DENSsolution, The Netherlands. The microchips had outer dimensions of 2.0×2.6×0.4 $mm^3$ and each contained a silicon nitride (SiN) membrane window with dimensions of 150×400 $\mu m^2$ along with a membrane of 50 nm thickness. Trivial transfer multilayer graphene was purchased from ACS Material, Pasadena, CA. $NaCl_2$ crystals were from Plano, Wetzlar, Germany.

### Cell culture and transfection for electrophysiological and biochemical experiments

An HEK293 cell line, stably expressing an ORAI1 N223A mutant, was created as described previously (Kilch et al., 2013). All cells were maintained in a 37°C, 5% $CO_2$ humidified incubator in corresponding medium, namely, minimum essential medium (MEM) for HEK293 wild type (HEKWT) and those stably expressing ORAI1 N223A (HEK N223A) or DMEM for HEK cells stably expressing STIM1 [HEKS1, courtesy of Jonathan Soboloff, Medical Genetics and Molecular Biochemistry, Temple University, USA (Soboloff et al., 2006)]. Media were supplemented with 10% fetal calf serum and 1% penicillin-streptomycin, with HEK N223A maintained in 1 µg/ml puromycin, while HEKS1 were maintained in 0.5 mg/ml G418. For electrophysiology and intracellular $Ca^{2+}$ measurements, cells were transfected with the indicated amount of DNA by electroporation with Nucleofector II (Lonza) according to the manufacturer's instructions. Alternatively, for biochemical experiments, cells were transfected with JetPei (PolyPlus) according to the manufacturer's instructions

### Generation of CRISPR/Cas9-mediated ORAI-knockout cell lines

Sequence-specific gRNA for the 5′-UTR *ORAI1* (5′-GTGAGGCCGGGC-CCGCGTAGGGG-3′) or within the coding sequence of *ORAI2* (5′-AGA-CGCAGTACCAGTACCCGCGG-3′) were designed using an online tool (http://crispr.dbcls.jp/). The corresponding plasmids were generated as described below and used for generation of the HEK CRI1 cell line. Alternatively, sequence-specific gRNA for *ORAI1–ORAI3*, as previously used (Zheng et al., 2018), were subcloned into pX459 [pSpCas9(BB)-2A-Puro V2.0, Addgene plasmid #62988]. This was done using the BbsI recognition site or in a modified vector backbone where the puromycin-resistance gene was replaced with either GFP or mCherry to allow simultaneous knockout of all three target genes and thereby generate the HEK CRI2 cell line. HEK293 cells were transfected with the generated CRISPR plasmids using JetPei (Polyplus) according to manufacturer's instructions. Cells showing both GFP and mCherry fluorescence were isolated by fluorescence-activated cell sorting (FACS, BD Aria III). The fluorescent cells were cultured in medium containing 1 µg/µl puromycin to allow for the selection of cells expressing all three plasmids. Monoclonal cell lines were generated by limiting dilution and knockout was verified by sequencing genomic DNA, western blotting for ORAI1 and intracellular $Ca^{2+}$ measurements (Fig. S1).

### Plasmids

Untagged ORAI1 was sub-cloned into pMAX containing GFP followed by P2A peptide (Kim et al., 2011). To create extracellularly tagged ORAI1, a PCR was conducted using two phosphorylated oligonucleotides (5′-GTAC-CGGATTACGCCCCCACCAGCAAGCCCCC-3′ and 3′-GCCAGGCCA-GCCAAGGTACCCATATGAC-5′) to add the hemagglutinin (HA) tag within the second extracellular loop of ORAI1 between the arginine (R210) and proline (P211) residues. To construct concatenated ORAI1 dimers, two oligonucleotides were designed to contain the linker sequence previously used by Zhou et al. (2015) (amino acids GGSGGSGGGILQSRGGSGGS-GGSG). The sequence was flanked by XhoI and BglII recognition sites, then introduced at the C-term of the first ORAI1 subunit. Eventually, the second ORAI1 subunit (with or without an HA tag) was added using the BglII recognition site. Using this strategy, we created untagged (O1–O1), double-tagged [(HA–O1)–(O1–HA)] and single-tagged [(HA–O1)–O1 and O1–(O1-HA)] constructs.

### Single cell $Ca^{2+}$ imaging

HEKS1 cells were transfected seeded on glass coverslips 24 h before measurements were conducted. On the measurement day, cells were loaded with 1 µM Fura 2-AM in medium at room temperature for 20–25 min. All experiments were performed in a self-built perfusion chamber with low volume and high solution exchange rate at room temperature (as in Alansary et al., 2015). The external $Ca^{2+}$ Ringer solution contained (in mM): 145 NaCl, 2 $MgCl_2$, 4 KCl, 10 glucose, 10 HEPES and 0.5 $CaCl_2$ (0.5 $Ca^{2+}$ Ringer) or no $CaCl_2$, but 1 EGTA (0 $Ca^{2+}$ Ringer) (pH 7.4 with NaOH). Images were analyzed with TILLVision followed by Igor software. For stimulation of store-operated $Ca^{2+}$ influx, 1 µM thapsigargin (Tg) was applied.

### Electrophysiology

Recordings from transfected HEKS1 were performed at room temperature in the tight-seal whole-cell configuration. Linear voltage ramps from

Journal of Cell Science (2020) 133, jcs240358. doi:10.1242/jcs.240358

−150 mV to +100 mV were applied as in Kilch et al. (2013). The pipette solution contained the following (in mM): 120 cesium-glutamate, 3 $MgCl_2$, 20 cesium-BAPTA, 10 HEPES and 0.05 $IP_3$ (pH 7.2 with CsOH). The bath solution contained (in mM): 120 NaCl, 10 TEA-Cl, 10 $CaCl_2$, 2 $MgCl_2$, 10 HEPES and glucose (pH 7.2 with NaOH).

### Western blotting

For protein expression analysis, cell pellets from HEK N223A were collected, frozen at −80°C until lysed in RIPA buffer containing 150 mM NaCl, 5 mM EDTA, 0.1% SDS, 0.5% sodium deoxycholate, 1% Nonidet P-40, 5 mM Tris-HCl, pH 8, supplemented with protease inhibitors (Complete EDTA-free, Roche). Proteins were denatured in Laemmli buffer at 65°C for 15 min under reducing conditions and, finally, standard SDS-PAGE was performed followed by electrotransfer to nitrocellulose membranes. Immunoblots were probed with anti-ORAI1 antibody (Sigma, catalog number O8264 at 1:1000). For protein detection, an enhanced chemiluminescence detection reagent was used (Clarity Western ECL Substrate, Bio-Rad). Densitometric quantification of detected protein bands was done with Quantity one software (Bio-Rad).

### ORAI1 cross-linking experiments

HEK N223A cells were harvested non-enzymatically using Tryp-LE (Thermo Fisher Scientific) according to the manufacturer's instructions. Cells were washed twice with cross-linking buffer (20 mM HEPES, 2 mM $Ca^{2+}$, pH 8) then resuspended in the same buffer containing 5 mM of the membrane permeable (DSP) or impermeable (BS3) cross-linkers prepared according to manufacturer's instructions (Thermo Fisher Scientific). Cells were incubated for 2 h on ice for cross-linking. Excess cross linker was removed by adding quenching buffer to a final concentration of 20 mM Tris-HCl, pH 7.5 and incubating at room temperature for a further 15 min. Finally, cells were lysed as mentioned above and protein probes were treated with non-reducing buffer for denaturation at 37°C for 30 min before they were analyzed by electrophoresis using pre-cast gradient gels (Novex, 4–12% Tris-Glycine Gels, Invitrogen). Immunoblots were probed with anti-HA antibody (clone 3F10, Roche, at 1:1000 dilution).

### Blue Native gel electrophoresis

HEK N223A or HEK CRI2 cells transfected with plasmid encoding dimeric ORAI1, were non-enzymatically harvested using Tryp-LE (Thermo Fisher Scientific). The lysing procedure involved incubation at 4°C for 30 min with shaking in a buffer containing 20 mM Tris-HCl pH 7.4, 100 mM NaCl, 10% glycerol and 2.5% n-octyl glucoside (Sigma-Aldrich) and protease inhibitors (Complete EDTA-free, Roche). A 6–16.5% gradient gel was prepared using a gradient mixer (Sigma-Aldrich) and overlaid by a 4% stacking gel. The gels were cast into a Hoeffer gel system (SE, 600 Series, Amersham Biosciences). Following electrophoresis, gels were blotted onto PVDF membrane using a semi-dry blotting system (Owl™ HEP Serie Semi-Dry-Elektroblotting-System, Thermo Fisher Scientific). Immunoblots were probed with anti-HA antibody as mentioned above.

### Surface protein biotinylation

For combined cross-linking and surface membrane biotinylation experiments, HEK N223A cells were treated with the cross-linkers as mentioned above. After quenching of excess cross-linker, cells were suspended in 2 mg/ml biotin-NHS-LC (Thermo Fisher Scientific) in cross-linker buffer and incubated at 4°C for 45 min. Unbound biotin was quenched with PBS containing 0.2 M glycine. Cells were lysed and biotinylated proteins were isolated using avidin beads as described in Alansary et al. (2015).

### Graphene transfer and preparation for liquid-phase electron microscopy

Polymer-covered multi-layer (three to five layers) graphene and poly-methyl-methacrylate (PMMA) was used to protect the sample during STEM. For the detachment of the graphene from the polymer substrate, the compound was plunged into a $NaCl_2$ saturated, deionized water solution at a 45° angle. The graphene–PMMA stack floated on the surface, and was scooped up with a 1×1 cm large $NaCl_2$ crystal (Plano, Germany) (Dahmke et al., 2017; Weatherup et al., 2016). The NaCl–graphene ensemble was baked in an oven at 100°C for 20 min. To remove the PMMA, it was immersed in acetone for 30 min and subsequently air dried. To cover the samples, the graphene on salt was cut into the desired size with a razor blade.

### Preparation of microchips with transfected HEK cells

CELLVIEW dishes and microchips with thin SiN windows were used as a support for HEK CRI1 cells. New microchips (Ring et al., 2011) contained a protective photoresist coating, which was removed with 2 min washes: first in acetone, then in ethanol. Afterwards, the microchips were briefly air-dried. Subsequently, both the pristine dishes and the microchips were plasma-cleaned for 5 min to render the glass and SiN surfaces hydrophilic. Immediately following this, they were incubated in 0.01% PLL for 5 min. After two rinses with HPLC grade water, the microchips were each placed in an individual well of a 96-well plate filled with cell medium that had been supplemented with 10% FBS and 50 µM 2-mercaptoethanol; these compartments were prefilled. Cells were grown in a 25 $cm^2$ cell culture flask and harvested when approaching 90% confluency by detaching them with 0.5 ml Cellstripper, waiting 5 min at room temperature, and diluting the cell suspension with 4.5 ml of cell medium supplemented with 10% FBS and 2-mercaptoethanol. This solution was centrifuged for 5 min (200 ***g***) and resuspended in 5 ml of cell medium supplemented with 10% FBS and 2-mercaptoethanol. Transfection of the cells was performed according the instructions of the supplier. Briefly, 80 µl transfection buffer (TRB), 0.25 µg DNA and 1.5 µl transfection reagent (TR), were mixed with 420 µl cell suspension in each dish compartment. For each prepared microchip, these volumes and amounts were divided by a factor of four. Prior to the settlement of the cells on the microchips and into the compartments, the microchips were placed into new wells filled with 20 µl of medium supplemented with 10% FCS and 50 µM 2-mercaptoethanol, and the dish compartments were emptied. Volumes of 100 µl, or 400 µl of cell suspension mixed with the DNA transfection solution were seeded onto the microchips and into the compartments. After 5 min, the cells had settled on the window area and the microchips were placed into the dishes on the rim besides the glass bottom area. The cell samples were then incubated for 24 h in the $CO_2$ incubator.

### Labeling of overexpressed ORAI1–HA

A two-step labeling protocol (Peckys et al., 2016; Peckys and de Jonge, 2015) was applied using a biotinylated anti-HA Fab, followed by labeling with QD565. At 24 h after transfection, the microchip samples were placed into wells pre-filled with cell medium supplemented with 10% FBS and 2-mercaptoethanol that had been warmed to 37°C. Then, the samples were rinsed briefly in pre-warmed 0.1 M cacodyl buffer containing 0.1 M sucrose, pH 7.4 (CB), followed by fixation with 3% formaldehyde and 0.2% glutaraldehyde in CB for 10 min at room temperature. This fixation protocol avoids the release of $Ca^{2+}$ from intracellular stores due to fixation artifacts (Kusumi and Suzuki, 2005). The cells in the dish compartments were processed similarly. After fixation, cells were rinsed once with CB and three times with PBS, then placed in GLY-PBS (0.1% glycine in PBS) for 2 min, followed by a rinse in PBS. The cells were then incubated in 400 ng/ml anti-HA-Fab–biotin labeling solution in PBS, first for 1 h at room temperature, followed by 3–6 h at 4°C. The QD-labeling solutions were prepared by first diluting 1 µM streptavidin-QD stock solutions at 1:5 in 40 mM borate buffer, pH 8.3, and a further dilution in BSA-PBS (PBS with 1% BSA) to obtain a 20 nM QD-labeling solution. The cells were rinsed three times in PBS, then incubated in the streptavidin–QD-labeling solution for 12 min at room temperature. Note that any BSA addition to the PBS buffer in the processing steps prior to the QD incubation led to a deterioration in the labeling results, leading to the formation of micron-sized fluorescent chunks after addition of the streptavidin-QD. Since no unspecific binding occurred without addition of BSA, it was omitted in the processing steps before the QD incubation. After the QD incubation, the cells were rinsed four times with BSA-PBS before fluorescence microscopy was performed, as explained in the following paragraph. To stabilize the cells for electron microscopy, the microchip samples were further fixed with 2% glutaraldehyde in CB for 10 min at room temperature. After one rinse with CB, and three rinses with BSA-PBS, the samples were stored in BSA-PBS supplemented with 0.02% sodium azide, at 4°C until liquid-phase STEM.

### Fluorescence microscopy

After the formaldehyde fixation, the HEK CRI1 cells with QD-labeled ORAI1–HA were imaged in an inverted fluorescence microscope (DMI6000B Leica, Germany). For this, microchips were placed upside-down in a pristine, 35 mm cell culture glass-bottom dish, without compartments, filled with 2 ml BSA-PBS. Cells on microchips were imaged with 20× and 40× objectives using direct interference contrast (DIC), and fluorescence filters specific for GFP (L5), QD655 (A) and QD565 (RHO) absorption and emission wavelengths. The imaging settings for each fluorescence signal were kept identical between different samples to allow for quantification. For quantification and control purposes, QD-labeled cells on the glass bottom of the CELLVIEW dishes were imaged similarly.

### Graphene coating and liquid-phase STEM

In order to keep the cell in a hydrated state during liquid-phase STEM, wet HEK CRI1 cells on the microchips were covered with graphene (Dahmke et al., 2017). This was performed by first cutting graphene on NaCl support crystals with a razor blade into a piece of desired size (~2×2 mm). Using the magnified view of a binocular, the graphene–NaCl crystal was held with tweezers and slowly submerged, with a 20–45° angle, in 100 ml of HPLC water in a glass beaker. Once contact was made with water, the graphene sheet quickly detached from the NaCl and floated on the water surface. It was carefully scooped up with the microchip sample, held by a fine, curved tweezer, and left to air-dry on the surface. Here, the cells enclosed between the graphene and SiN membrane of the microchip still remained hydrated.

The cells were then imaged in a transmission electron microscope (TEM; ARM 200, JEOL, Japan), using STEM in dark-field mode to observe the individual QD-labeled ORAI1–HA positions (Dahmke et al., 2017). The imaging settings were as follows: electron energy of 200 kV, spot size setting 2C, aperture size 20 µm, and 175 pA probe current. First, an overview of the STEM images of the sample and entire SiN window were acquired, then compared to the previously recorded fluorescence and DIC images. This correlative method allowed for quick relocation of the cells during electron microscopy, as well as choosing representative cells for the high-resolution STEM imaging. High-resolution images of cells with labels were acquired with pixel dwell-times ranging between 10 and 14 µs, a magnification of 60,000× for imaging QD655 and of 120,000× for imaging QD565, yielding pixel sizes of 1.7×1.7 nm and 0.8×0.8 nm, respectively. The image size of the 16-bit images was 2048×2048 pixels, comprising scanning areas of 11.7 $\mu m^2$ and 2.89 $\mu m^2$, respectively, per image. The calculated electron doses ranged between 16 and 253 $e^-/Å^2$, thus lying within the known limit of radiation damage (Hermannsdörfer et al., 2016).

### Particle detection

STEM images were analyzed to obtain the lateral coordinates of the QD labels. All images were visually checked prior to automated particle detection. Occasionally, contaminants resided on the graphene originating from residues of the production process. Such contaminants produced STEM contrast hindering automated label detection. These small artifacts came in a variety of sizes, shapes and contrast values making them distinguishable from the highly uniform size, shape and contrast value of the QD labels. In cases where the contaminants interfered with the automatic label detection, contaminants were manually removed from the image by covering them with a fitting round or oval shape, filled with the gray value of the surrounding background, using ImageJ (NIH). To detect the QD labels and determine their center positions, a local design Plugin in ImageJ was applied as described in detail elsewhere (Peckys et al., 2015). This software is available on request to the corresponding author. Briefly, a Fourier filter was adjusted for the passage of spatial frequencies between a factor of 3 smaller and a factor of 3 higher than the average QD size, 8 nm. The image was then binarized using an automated threshold with a maximum entropy setting. Finally, the particles were automatically detected using the 'Analyze Particles' tool that selects particles with an area within a factor of 2 of the expected area. The precision of the particle detection amounted to the pixel size of 0.8 nm for images with QD565 and 1.6 nm for images with QD655.

The $g(r)$ function yields the probability of finding the center of a particle at a given distance from the center of any other particle, ultimately demonstrating if the particles are distributed by chance or if an underlying reason for the preferred occurrence of distances deviating from randomness is present.

### Quantitative fluorescence measurements

To compare the relative QD-labeling efficiencies between different ORAI1–HA proteins, the mean fluorescence intensity was measured for both the GFP and the QD565 fluorescence channels of QD-labeled HEK CRI1 cells. For this, a round or oval region of interest (ROI) was drawn on all transfected cells, which were visible in the light microscopic image recorded from a randomly chosen area. Each ROI comprised 25–75% of the total adherence area of the underlying cell, which was deemed sufficient, as both fluorescence signals showed quite uniform cellular distributions. From these individual cellular fluorescence intensity values, a background correction was performed by subtracting the mean background fluorescence value determined from an area with unsuccessfully transfected cells lying in the vicinity of the respective cell. The corrected mean intensity values of the QD channel of all measured cells were plotted against their corresponding corrected GFP intensities. The resulting regression line was calculated for each experimental group using Excel.

#### Acknowledgements

We thank Anja Bergsträßer and Elmar Krause from the FACS facility of the Institute of Physiology, Maylin Merino-Wong for help with cell sorting, Kathrin Förderer for technical assistance, Sercan Keskin, and Peter Kunnas for help with the STEM, E. Arzt for his support through INM, and Dr K. von der Malsburg and Dr van der Laan for their support with the Blue Native gel experiments.

#### Competing interests

The authors declare no competing or financial interests.

#### Author contributions

Conceptualization: N.d.J., B.A.N., D.A., D.B.P.; Methodology: D.A., D.B.P.; Software: N.d.J.; Validation: D.A., D.B.P.; Formal analysis: N.d.J., B.A.N., D.A., D.B.P.; Investigation: D.A., D.B.P.; Resources: N.d.J., B.A.N.; Writing - original draft: N.d.J., B.A.N., D.A., D.B.P.; Writing - review & editing: N.d.J., B.A.N., D.A., D.B.P.; Visualization: D.A., D.B.P.; Supervision: N.d.J., B.A.N.; Project administration: N.d.J., B.A.N.; Funding acquisition: N.d.J., B.A.N.

#### Funding

The research was funded by the Deutsche Forschungsgemeinschaft [SFB1027 (project C7), FOR2289 to B.A.N. and D.A.].

#### Supplementary information

Supplementary information available online at
http://jcs.biologists.org/lookup/doi/10.1242/jcs.240358.supplemental

#### References

**Alansary, D., Bogeski, I. and Niemeyer, B. A.** (2015). Facilitation of Orai3 targeting and store-operated function by Orai1. *Biochim. Biophys. Acta* **1853**, 1541-1550. doi:10.1016/j.bbamcr.2015.03.007

**Alansary, D., Schmidt, B., Dörr, K., Bogeski, I., Rieger, H., Kless, A. and Niemeyer, B. A.** (2016). Thiol dependent intramolecular locking of Orai1 channels. *Sci. Rep.* **6**, 33347. doi:10.1038/srep33347

**Bergmeier, W., Weidinger, C., Zee, I. and Feske, S.** (2013). Emerging roles of store-operated $Ca^{2+}$ entry through STIM and ORAI proteins in immunity, hemostasis and cancer. *Channels (Austin)* **7**, 379-391. doi:10.4161/chan.24302

**Cai, X., Zhou, Y., Nwokonko, R. M., Loktionova, N. A., Wang, X., Xin, P., Trebak, M., Wang, Y. and Gill, D. L.** (2016). The Orai1 store-operated calcium channel functions as a Hexamer. *J. Biol. Chem.* **291**, 25764-25775. doi:10.1074/jbc.M116.758813

**Dahmke, I. N., Verch, A., Hermannsdörfer, J., Peckys, D. B., Weatherup, R. S., Hofmann, S. and de Jonge, N.** (2017). Graphene liquid enclosure for single-molecule analysis of membrane proteins in whole cells using electron microscopy. *ACS Nano* **11**, 11108-11117. doi:10.1021/acsnano.7b05258

**De Jonge, N.** (2018). Membrane protein stoichiometry studied in intact mammalian cells using liquid-phase electron microscopy. *J. Microsc.* **269**, 134-142. doi:10.1111/jmi.12570

**de Jonge, N. and Ross, F. M.** (2011). Electron microscopy of specimens in liquid. *Nat. Nanotechnol.* **6**, 695-704. doi:10.1038/nnano.2011.161

**Demuro, A., Penna, A., Safrina, O., Yeromin, A. V., Amcheslavsky, A., Cahalan, M. D. and Parker, I.** (2011). Subunit stoichiometry of human Orai1 and Orai3 channels in closed and open states. *Proc. Natl. Acad. Sci. USA* **108**, 17832-17837. doi:10.1073/pnas.1114814108

**Dolmetsch, R.** (2003). Excitation-transcription coupling: signaling by ion channels to the nucleus. *Sci. STKE* **2003**, PE4. doi:10.1126/scisignal.1662003pe4
**Dörr, K., Kilch, T., Kappel, S., Alansary, D., Schwär, G., Niemeyer, B. A. and Peinelt, C.** (2016). Cell type-specific glycosylation of Orai1 modulates store-operated $Ca^{2+}$ entry. *Sci. Signal.* **9**, ra25. doi:10.1126/scisignal.aaa9913
**Fahrner, M., Schindl, R. and Romanin, C.** (2018). Studies of structure-function and subunit composition of Orai/STIM channel. In *Calcium Entry Channels in Non-Excitable Cells* (ed. J. A. Kozak and J. W. PutneyJr), pp. 25-50. CRC Press/Taylor & Francis, Boca Raton, FL.
**Gurevich, V. V. and Gurevich, E. V.** (2018). GPCRs and signal transducers: interaction stoichiometry. *Trends Pharmacol. Sci.* **39**, 672-684. doi:10.1016/j.tips.2018.04.002
**Gwack, Y., Srikanth, S., Feske, S., Cruz-Guilloty, F., Oh-hora, M., Neems, D. S., Hogan, P. G. and Rao, A.** (2007). Biochemical and functional characterization of Orai proteins. *J. Biol. Chem.* **282**, 16232-16243. doi:10.1074/jbc.M609630200
**Hermannsdörfer, J., Tinnemann, V., Peckys, D. B. and de Jonge, N.** (2016). The effect of electron beam irradiation in environmental scanning transmission electron microscopy of whole cells in liquid. *Microsc. Microanal.* **22**, 656-665. doi:10.1017/S1431927616000763
**Hoth, M. and Niemeyer, B. A.** (2013). The neglected CRAC proteins: Orai2, Orai3, and STIM2. *Curr. Top. Membr.* **71**, 237-271. doi:10.1016/B978-0-12-407870-3.00010-X
**Hou, M.-F., Kuo, H.-C., Li, J.-H., Wang, Y.-S., Chang, C.-C., Chen, K.-C., Chen, W.-C., Chiu, C.-C., Yang, S. and Chang, W.-C.** (2011). Orai1/CRACM1 overexpression suppresses cell proliferation via attenuation of the store-operated calcium influx-mediated signalling pathway in A549 lung cancer cells. *Biochim. Biophys. Acta* **1810**, 1278-1284. doi:10.1016/j.bbagen.2011.07.001
**Hou, X., Pedi, L., Diver, M. M. and Long, S. B.** (2012). Crystal structure of the calcium release-activated calcium channel Orai. *Science* **338**, 1308-1313. doi:10.1126/science.1228757
**Hou, X., Burstein, S. R. and Long, S. B.** (2018). Structures reveal opening of the store-operated calcium channel Orai. *eLife* **7**, e36758. doi:10.7554/eLife.36758
**Howarth, M., Liu, W., Puthenveetil, S., Zheng, Y., Marshall, L. F., Schmidt, M. M., Wittrup, K. D., Bawendi, M. G. and Ting, A. Y.** (2008). Monovalent, reduced-size quantum dots for imaging receptors on living cells. *Mat. Meth.* **5**, 397-399. doi:10.1038/nmeth.1206
**Ji, W., Xu, P., Li, Z., Lu, J., Liu, L., Zhan, Y., Chen, Y., Hille, B., Xu, T. and Chen, L.** (2008). Functional stoichiometry of the unitary calcium-release-activated calcium channel. *Proc. Natl. Acad. Sci. USA* **105**, 13668-13673. doi:10.1073/pnas.0806499105
**Kar, P. and Parekh, A.** (2013). STIM proteins, Orai1 and gene expression. *Channels (Austin)* **7**, 374-378. doi:10.4161/chan.25298
**Kilch, T., Alansary, D., Peglow, M., Dörr, K., Rychkov, G., Rieger, H., Peinelt, C. and Niemeyer, B. A.** (2013). Mutations of the $Ca^{2+}$-sensing stromal interaction molecule STIM1 regulate $Ca^{2+}$ influx by altered oligomerization of STIM1 and by destabilization of the $Ca^{2+}$ channel Orai1. *J. Biol. Chem.* **288**, 1653-1664. doi:10.1074/jbc.M112.417246
**Kim, J. H., Lee, S.-R., Li, L.-H., Park, H.-J., Park, J.-H., Lee, K. Y., Kim, M.-K., Shin, B. A. and Choi, S.-Y.** (2011). High cleavage efficiency of a 2A peptide derived from porcine teschovirus-1 in human cell lines, zebrafish and mice. *PLoS ONE* **6**, e18556. doi:10.1371/journal.pone.0018556
**Kusumi, A. and Suzuki, K.** (2005). Toward understanding the dynamics of membrane-raft-based molecular interactions. *Biochim. Biophys. Acta* **1746**, 234-251. doi:10.1016/j.bbamcr.2005.10.001
**Li, P., Miao, Y., Dani, A. and Vig, M.** (2016). alpha-SNAP regulates dynamic, on-site assembly and calcium selectivity of Orai1 channels. *Mol. Biol. Cell* **27**, 2542-2553. doi:10.1091/mbc.e16-03-0163
**Liu, X., Wu, G., Yu, Y., Chen, X., Ji, R., Lu, J., Li, X., Zhang, X., Yang, X. and Shen, Y.** (2019). Molecular understanding of calcium permeation through the open Orai channel. *PLoS Biol.* **17**, e3000096. doi:10.1371/journal.pbio.3000096
**Madl, J., Weghuber, J., Fritsch, R., Derler, I., Fahrner, M., Frischauf, I., Lackner, B., Romanin, C. and Schütz, G. J.** (2010). Resting state Orai1 diffuses as homotetramer in the plasma membrane of live mammalian cells. *J. Biol. Chem.* **285**, 41135-41142. doi:10.1074/jbc.M110.177881
**Maruyama, Y., Ogura, T., Mio, K., Kato, K., Kaneko, T., Kiyonaka, S., Mori, Y. and Sato, C.** (2009). Tetrameric Orai1 is a teardrop-shaped molecule with a long, tapered cytoplasmic domain. *J. Biol. Chem.* **284**, 13676-13685. doi:10.1074/jbc.M900812200
**Maruyama, Y., Ebihara, T., Nishiyama, H., Suga, M. and Sato, C.** (2012). Immuno EM-OM correlative microscopy in solution by atmospheric scanning electron microscopy (ASEM). *J. Struct. Biol.* **180**, 259-270. doi:10.1016/j.jsb.2012.08.006
**Mignen, O., Thompson, J. L. and Shuttleworth, T. J.** (2008). Both Orai1 and Orai3 are essential components of the arachidonate-regulated $Ca^{2+}$-selective (ARC) channels. *J. Physiol.* **586**, 185-195. doi:10.1113/jphysiol.2007.146258
**Nwokonko, R. M., Cai, X., Loktionova, N. A., Wang, Y., Zhou, Y. and Gill, D. L.** (2017). The STIM-Orai pathway: conformational coupling between STIM and Orai in the activation of store-operated $Ca^{2+}$ entry. *Adv. Exp. Med. Biol.* **993**, 83-98. doi:10.1007/978-3-319-57732-6_5
**Park, C. Y., Hoover, P. J., Mullins, F. M., Bachhawat, P., Covington, E. D., Raunser, S., Walz, T., Garcia, K. C., Dolmetsch, R. E. and Lewis, R. S.** (2009). STIM1 clusters and activates CRAC channels via direct binding of a cytosolic domain to Orai1. *Cell* **136**, 876-890. doi:10.1016/j.cell.2009.02.014
**Peckys, D. B. and de Jonge, N.** (2014). Liquid scanning transmission electron microscopy: imaging protein complexes in their native environment in whole eukaryotic cells. *Microsc. Microanal.* **20**, 346-365. doi:10.1017/S1431927614000099
**Peckys, D. B. and de Jonge, N.** (2015). Studying the stoichiometry of epidermal growth factor receptor in intact cells using correlative microscopy. *J. Vis. Exp.* **103**, e53186. doi:10.3791/53186
**Peckys, D. B., Korf, U. and de Jonge, N.** (2015). Local variations of HER2 dimerization in breast cancer cells discovered by correlative fluorescence and liquid electron microscopy. *Sci. Adv.* **1**, e1500165. doi:10.1126/sciadv.1500165
**Peckys, D. B., Alansary, D., Niemeyer, B. A. and de Jonge, N.** (2016). Visualizing quantum dot labeled ORAI1 proteins in intact cells via correlative light and electron microscopy. *Microsc. Microanal.* **22**, 902-912. doi:10.1017/S1431927616011491
**Penna, A., Demuro, A., Yeromin, A. V., Zhang, S. L., Safrina, O., Parker, I. and Cahalan, M. D.** (2008). The CRAC channel consists of a tetramer formed by Stim-induced dimerization of Orai dimers. *Nature* **456**, 116-120. doi:10.1038/nature07338
**Prakriya, M. and Lewis, R. S.** (2015). Store-operated calcium channels. *Phys. Rev.* **95**, 1383-1436. doi:10.1152/physrev.00020.2014
**Qiu, R. and Lewis, R. S.** (2019). Structural features of STIM and Orai underlying store-operated calcium entry. *Curr. Opin. Cell Biol.* **57**, 90-98. doi:10.1016/j.ceb.2018.12.012
**Ring, E. A., Peckys, D. B., Dukes, M. J., Baudoin, J. P. and de Jonge, N.** (2011). Silicon nitride windows for electron microscopy of whole cells. *J. Microsc.* **243**, 273-283. doi:10.1111/j.1365-2818.2011.03501.x
**Robinson, J. M., Takizawa, T. and Vandré, D. D.** (2000). Enhanced labeling efficiency using ultrasmall immunogold probes: Immunocytochemistry. *J. Histochem. Cytochem.* **48**, 487-492. doi:10.1177/002215540004800406
**Schmidt, B., Alansary, D., Bogeski, I., Niemeyer, B. A. and Rieger, H.** (2019). Reaction-diffusion model for STIM-ORAI interaction: The role of ROS and mutations. *J. Theor. Biol.* **470**, 64-75. doi:10.1016/j.jtbi.2019.02.010
**Soboloff, J., Spassova, M. A., Hewavitharana, T., He, L.-P., Xu, W., Johnstone, L. S., Dziadek, M. A. and Gill, D. L.** (2006). STIM2 is an inhibitor of STIM1-mediated store-operated Ca2+ Entry. *Curr. Biol.* **16**, 1465-1470. doi:10.1016/j.cub.2006.05.051
**Stoyan, D. and Stoyan, H.** (1996). Estimating pair correlation functions of planar cluster processes. *Biom. J.* **38**, 259-271. doi:10.1002/bimj.4710380302
**Weatherup, R. S., Shahani, A. J., Wang, Z.-J., Mingard, K., Pollard, A. J., Willinger, M.-G., Schloegl, R., Voorhees, P. W. and Hofmann, S.** (2016). In situ Graphene growth dynamics on polycrystalline catalyst foils. *Nano Lett.* **16**, 6196-6206. doi:10.1021/acs.nanolett.6b02459
**Yen, M. and Lewis, R. S.** (2019). Numbers count: How STIM and Orai stoichiometry affect store-operated calcium entry. *Cell Calcium* **79**, 35-43. doi:10.1016/j.ceca.2019.02.002
**Yen, M., Lokteva, L. A. and Lewis, R. S.** (2016). Functional analysis of Orai1 concatemers supports a hexameric stoichiometry for the CRAC channel. *Biophys. J.* **111**, 1897-1907. doi:10.1016/j.bpj.2016.09.020
**Yuan, J. P., Zeng, W., Dorwart, M. R., Choi, Y.-J., Worley, P. F. and Muallem, S.** (2009). SOAR and the polybasic STIM1 domains gate and regulate Orai channels. *Nat. Cell Biol.* **11**, 337-343. doi:10.1038/ncb1842
**Zheng, S., Zhou, L., Ma, G., Zhang, T., Liu, J., Li, J., Nguyen, N. T., Zhang, X., Li, W., Nwokonko, R. et al.** (2018). Calcium store refilling and STIM activation in STIM- and Orai-deficient cell lines. *Pflugers Arch.* **470**, 1555-1567. doi:10.1007/s00424-018-2165-5
**Zhou, Y., Wang, X., Loktionova, N. A., Cai, X., Nwokonko, R. M., Vrana, E., Wang, Y., Rothberg, B. S. and Gill, D. L.** (2015). STIM1 dimers undergo unimolecular coupling to activate Orai1 channels. *Nat. Commun.* **6**, 8395. doi:10.1038/ncomms9395